ELSEVIER

Physics Letters A 306 (2002) 25–34

PHYSICS LETTERS A

www.elsevier.com/locate/pla

A numerical study of the semi-classical limit of the focusing nonlinear Schrödinger equation

H.D. Ceniceros [a], Fei-Ran Tian [b,*]

[a] *Department of Mathematics, University of California, Santa Barbara, CA 93106, USA*
[b] *Department of Mathematics, The Ohio State University, Columbus, OH 43210, USA*

Received 10 July 2000; received in revised form 8 December 2000; accepted 11 December 2000

Communicated by A.P. Fordy

Abstract

We study the solution of the focusing nonlinear Schrödinger equation in the semiclassical limit. Numerical solutions are presented for four different kinds of initial data, of which three are analytic and one is nonanalytic. We verify numerically the weak convergence of the oscillatory solution by examining the strong convergence of the spatial average of the solution.

1. Introduction

Many dynamics in nature undergo dispersive processes, while the dissipative or diffusive mechanisms are negligible [23,30]. Examples include the vortex sheet problem of incompressible fluids [16], plasmas [13,27], and certain aspects of nonlinear optics [11, 20]. When the dispersive parameter is small, there appear regions in space–time which are filled with small scale oscillations. Such phenomena have been observed in collisionless shocks in plasmas [13] and optical shocks in optical fibers [20,26]. A consistent description of these nonlinear dispersive oscillations is rather complicated. So far, it has only been possible to study those oscillations governed by completely integrable systems.

There are two types of nonlinear dispersive equations with small dispersion. The first type is given by dispersive approximations of hyperbolic equations. Examples, both integrable and nonintegrable, are ample: the KdV equation [9,22], the generalized KdV equation [8], the defocusing nonlinear Schrödinger equation [10,11,17,18,20,28], Toda lattice [1,6] and other dispersive difference schemes [15,23]. Numerical experiments reveal, and analysis confirms by proof in some integrable cases, that the zero dispersion limit exists in the weak, i.e., average, sense. Furthermore, the weak limit dynamics, complicated though it is, is hyperbolic [7,23].

The second type consists of "nearly unstable" nonlinear dispersive equations; they are in the form of dispersive approximations of those evolution equations whose initial value problems are not well-posed. An important example is the well-known vortex sheet

* Corresponding author.
E-mail addresses: hdc@math.ucsb.edu (H.D. Ceniceros), tian@math.ohio-state.edu (F.-R. Tian).

0375-9601/02/$ – see front matter
PII: S0375-9601(01)00011-1

problem in inviscid incompressible fluid dynamics. When surface tension is absent, a vortex sheet is governed by the Birkhoff–Rott integral equation whose initial value problem is ill-posed [5,16]. This ill-posedness is caused by the Kelvin–Helmholtz instability. When surface tension is present, the evolution of the vortex sheet is described by a dispersive approximation of the Birkhoff–Rott equation with surface tension as the small dispersion [16]. Small scale oscillations (capillary waves) are observed in the curvature of the vortex sheet when surface tension is small but nonzero. These oscillations are responsible for the roll-over phenomenon on vortex sheets.

Another example is the focusing nonlinear Schrödinger equation (NLS) with small dispersion [31]. This focusing NLS can be written as a dispersive approximation of elliptic Euler equations [2,17,25]. The ellipticity gives rise to the Benjamin–Feir or modulational instability.

The focusing NLS has applications in many areas of sciences and technology. It has been used to describe the motion of a vortex filament in incompressible fluids [14], and to model the fractal fiber architecture of aortic heart valve leaflets in the study of the human heart [24].

There are very few analytical and numerical results concerning oscillations generated by "nearly unstable" nonlinear dispersive equations. In this Letter, we study an integrable model of this type of oscillations. Our obvious choice is the focusing NLS [31]. More precisely, we study the solution of the following initial value problem in the limit $\epsilon \to 0$:

$$i\epsilon\partial_t\psi + \frac{1}{2}\epsilon^2\partial_{xx}^2\psi + |\psi|^2\psi = 0, \tag{1}$$

with the initial data

$$\psi(x,0) = A_0(x)e^{(i/\epsilon)S_0(x)}, \tag{2}$$

for small ϵ, where $A_0(x)$ is the initial amplitude and $S_0(x)$ the real initial phase.

Recently, Miller and Kamvissis have cleverly made use of an exact solution of the focusing NLS [25]. This exact solution has an initial data of form (2):

$$A_0(x) = 2\,\mathrm{sech}(x), \qquad S_0(x) = 0. \tag{3}$$

By numerically studying this exact solution for $\epsilon = 0.4,\ 0.2,\ 0.1$, they observed some persistent patterns for small dispersion parameters. This suggests the existence of some kind of weak limits. However, no other exact solutions whose initial data has the form of (2) are known to exist. Thus, it becomes desirable to directly compute the solution of the focusing NLS for small dispersion.

In this Letter, we present some numerical computations of the solution of the focusing NLS when ϵ is small. This computational problem is notoriously difficult. Numerical studies of the usual zero dispersion limits of nonlinear dispersive equations are hampered by the fact that in order to resolve the dispersive term in the equations for a tiny value of dispersion parameter, it requires a much tinier value of Δx [23]. What makes the focusing NLS much more difficult than other dispersive equations, such as the KdV equation, is the modulational instability. However, we are able to resolve the numerics for values of epsilon as small as 0.00625. For each initial data that we experimented, smooth and oscillatory regions are observed and they seem to be independent of small ϵ. Within the oscillatory regions, the oscillations appear to be quite regular even when ϵ becomes smaller and smaller. The velocity and amplitude of the soliton in the oscillations can be predicted by the location of the eigenvalues of the Zakharov–Shabat operator. By computing the spatial average of the solution, we find strong evidence for the weak convergence of the semi-classical limit of the focusing NLS. These numerical observations are consistent with those of Miller and Kamvissis on the pure soliton solution. They are also in good agreement with those of Bronski and Kutz [4], who studied the behavior of solitons in the focusing NLS for $\epsilon = 0.1$.

The organization of this Letter is as follows. In Section 2, we present some analysis of the equation. We discuss the eigenvalue problem and relation of eigenvalues to the speed and amplitude of solitons. In Section 3, we develop a numerical scheme to compute the focusing NLS solution with small ϵ. In Section 4, we discuss the numerical results, with four kinds of initial data: zero initial phase data, symmetric and nonsymmetric data with nonzero initial phase, nonanalytic initial data. The main phenomena are pointed out: the existence of smooth and oscillatory regions and their propagation in space and time, the observation of regular patterns and weak convergence in the oscillatory region. Conclusions are given in Section 5.

2. Analysis of equations

The focusing NLS has infinitely many conservation laws. The first two are

$$\rho_t + \mu_x = 0, \tag{4}$$

$$\mu_t + \left[\frac{\mu^2}{\rho} - \frac{\rho^2}{2}\right]_x = \frac{\epsilon^2}{4}\left[\rho(\log\rho)_{xx}\right]_x, \tag{5}$$

where $\rho = |\psi|^2$ and $\mu = -i(\epsilon/2)(\bar{\psi}\psi_x - \psi\bar{\psi}_x)$. Here the bar denotes complex conjugate.

To describe the solution when ϵ is small, one formally sets $\epsilon = 0$. The resulting equations (4), (5), after substitution $\mu = \rho v$, become

$$\rho_t + (\rho v)_x = 0, \tag{6}$$

$$(\rho v)_t + \left[\rho v^2 - \frac{\rho^2}{2}\right]_x = 0. \tag{7}$$

These equations have characteristics $v \pm i\sqrt{\rho}$ and thus are elliptic when $\rho \neq 0$. They are exactly the Euler equations of one-dimensional gas dynamics with mass density ρ, velocity v and a strange pressure law $P = -\rho^2/2$. Since $dP/d\rho < 0$, the pressure decreases as the density increases, and we have a gas that likes to clump together around local density variations [2].

The initial value problems for Eqs. (4), (5) are well-posed for $\epsilon > 0$ and ill-posed for $\epsilon = 0$ when $\rho \neq 0$. It is therefore not obvious whether the solution of Eqs. (4), (5) has any reasonable limit as ϵ goes to zero.

One may attempt to solve the focusing NLS for each ϵ using the inverse scattering method and then let ϵ tend to zero. The solution of Eq. (1) begins with the spectrum for the Zakharov–Shabat operator,

$$L = \begin{pmatrix} i\epsilon\frac{\partial}{\partial x} & i\bar{\psi} \\ i\psi & -i\epsilon\frac{\partial}{\partial x} \end{pmatrix}.$$

This operator is not self-adjoint and its eigenvalues can virtually be any complex number except real [31]. The number of the eigenvalues tends to infinity as ϵ goes to zero. This makes the study of the spectrum of L extremely difficult for small ϵ [3].

It is known that each soliton of Eq. (1) corresponds to a complex eigenvalue $\xi + i\eta$ of L [31]. The real and imaginary parts of the eigenvalue are twice the speed and height of the soliton, respectively. Since eigenvalues may have the same real part, we can have a bundle of solitons traveling at exactly the same speed. That means that some solitons may not separate from one another. This phenomenon makes it difficult to analyze and compute the semi-classical limit of the focusing NLS.

We next analyze, in more detail, the eigenvalues of L when the initial data (1) has zero phase, i.e., $S_0(x) = 0$. Since it is isospectral, we only need to study L at the initial time. Calculating the square of L, we obtain

$$L^2 = \begin{pmatrix} -\epsilon^2\frac{\partial}{\partial x}^2 - |\psi|^2 & -\epsilon\bar{\psi}_x \\ \epsilon\psi_x & -\epsilon^2\frac{\partial}{\partial x}^2 - |\psi|^2 \end{pmatrix}.$$

Since $S_0(x) = 0$, the off-diagonal term

$$\epsilon\psi_x = [\epsilon A_{0x} + iA_{0x}S_{0x}]e^{iS_0/\epsilon} = \epsilon A_{0x}$$

goes to zero as $\epsilon \to 0$. Accordingly, L^2 behaves, when ϵ is tiny, like a linear Schrödinger operator with $|\psi(x,t)|^2$ as the potential function. The eigenvalues of L are thus almost pure imaginary for small ϵ.

For these initial data, further WKB studies show that the number of eigenvalues is of order $O(1/\epsilon)$ and that the reflection coefficients are exponentially small in ϵ. Roughly speaking, these data generate as many as order $O(1/\epsilon)$ solitons for small ϵ. Since the eigenvalues are almost pure imaginary, these solitons have negligible speed for tiny ϵ and are not expected to separate from one another.

In particular, for the initial data (3) studied by Miller and Kamvissis, all the eigenvalues are exactly pure imaginary and reflection coefficients are also exactly zero when ϵ takes values from a sequence $\{2/n\}$. This initial data generates the so called pure soliton solutions and they are given by exact formulae. Recently, Kamvissis, McLaughlin, and Miller have embarked on the task of analyzing these soliton solutions for small dispersion [19].

3. Numerical method

We describe now the numerical method we employ to compute directly the solution of the initial value problem for the focusing NLS.

The numerical computation of the NLS solution for small values of the parameter ϵ is a challenging problem. First, the solution is known to develop rapidly a "sea" of solitons whose wavelength is $O(\epsilon)$. Thus, as ϵ is decreased the length scale shrinks and very high resolution is required to compute the solution accurately.

Second, because the underlying initial value problem with zero dispersion is ill-posed, there is great sensitivity to round-off error noise when ϵ is sufficiently small. If left uncontrolled, the initially small round-off noise can quickly grow and destroy the accuracy of the computations.

Nonlinear Fourier filtering [21] has proved to be very useful to control the growth of the round-off error in the computation of nearly ill-posed problems. Here, we combine Fourier filtering with de-aliasing smoothing and a semi-implicit time discretization to obtain an efficient numerical method for the focusing NLS.

To describe our method we begin by writing $\psi = u + iv$, where u and v are real-valued functions. Then, the NLS for ψ is equivalent to the following system of equations:

$$u_t = -\frac{1}{2}\epsilon v_{xx} - \frac{1}{\epsilon}\left(u^2 + v^2\right)v, \tag{8}$$

$$v_t = \frac{1}{2}\epsilon u_{xx} + \frac{1}{\epsilon}\left(u^2 + v^2\right)u. \tag{9}$$

All the sets of initial data we consider here decay to zero fast as $|x| \to \infty$ and the corresponding time evolving solutions concentrate rapidly on a small interval. However, to avoid boundary effects, we compute the solution on a sufficiently large interval $[-M, M]$. Here we take $M = 10$.

Our numerical scheme for (8), (9) can be written as follows:

$$\frac{u_j^{n+1} - u_j^{n-1}}{2\Delta t} = -\frac{1}{4}\epsilon S_h^2 v_j^{n+1} - \frac{1}{4}\epsilon D_h^2 v_j^{n-1} - \frac{1}{\epsilon}\left[\left(u_j^n\right)^2 + \left(v_j^n\right)^2\right]v_j^n, \tag{10}$$

$$\frac{v_j^{n+1} - v_j^{n-1}}{2\Delta t} = \frac{1}{4}\epsilon S_h^2 u_j^{n+1} + \frac{1}{4}\epsilon D_h^2 u_j^{n-1} + \frac{1}{\epsilon}\left[\left(u_j^n\right)^2 + \left(v_j^n\right)^2\right]u_j^n, \tag{11}$$

where u_j^n and v_j^n denote the approximation of the solution at $t = n\Delta t$ and $x = -M + jh$ with $h = 2M/N$. N is the total number of grid points. Here S_h stands for the pseudo-spectral derivative approximation. That is, $\widehat{S_h f}_k = -i(\pi/M)k\hat{f}_k$, where $\hat{f}_k$ denotes the discrete Fourier transform of f. Because aliasing instabilities can commonly occur over long time computations, we have introduced in our method a smoothed pseudo-spectral derivative D_h. It is defined in Fourier space as $\widehat{D_h f}_k = -i(\pi/M)kr(kh)\hat{f}_k$, where $r(x)$ is a smooth cutoff function. The role of $r(x)$ is to damp the highest modes to suppress aliasing. Here, we use $r(x) = e^{-10(x/2M)^{25}}$.

Note that the smoothing filtering is used in the explicit derivative terms but not in the implicit ones. This selective filtering is important to maintain the regularizing effects at high modes for small ϵ. This is more clearly seen when we invert system (10), (11) in Fourier space:

$$\hat{u}_k^{n+1} = \frac{\hat{P}_k + (1/2)\Delta t\epsilon(\pi k/M)^2\hat{Q}_k}{1 + (1/4)(\Delta t)^2\epsilon^2(\pi k/M)^4}, \tag{12}$$

$$\hat{v}_k^{n+1} = \frac{\hat{Q}_k - (1/2)\Delta t\epsilon(\pi k/M)^2\hat{P}_k}{1 + (1/4)(\Delta t)^2\epsilon^2(\pi k/M)^4}, \tag{13}$$

where $\hat{P}_k$ and $\hat{Q}_k$ are the Fourier transforms of

$$P_j = u_j^{n-1} - \frac{\Delta t}{2}\epsilon D_h^2 v_j^{n-1} - \frac{2\Delta t}{\epsilon}\left[\left(u_j^n\right)^2 + \left(v_j^n\right)^2\right]v_j^n,$$

$$Q_j = v_j^{n-1} + \frac{\Delta t}{2}\epsilon D_h^2 u_j^{n-1} + \frac{2\Delta t}{\epsilon}\left[\left(u_j^n\right)^2 + \left(v_j^n\right)^2\right]u_j^n.$$

Smoothing filtering in the implicit derivative terms would modify the denominator of (12), (13) to become $1 + (1/4)(\Delta t)^2\epsilon^2 r^4(kh)(\pi k/M)^4$. Thus, the additional factor $r^4(kh)$ would suppress the high frequency regularization.

In addition to the smoothing filter, we also apply Fourier filtering to the solution at each time step. That is, we set to zero all the solution Fourier modes whose magnitudes are below a certain filter level. Here, we take the filter level to be 10^{-12} as all our computations are performed with double precision arithmetic.

Scheme (10), (11) is a second-order discretization in time of Crank–Nicholson type. The formal accuracy in space is $O(h^{25})$ because of the smoothing filter. A spectrally accurate filter is also possible but we did not implement it here.

For smooth solutions, the formal accuracy is confirmed for short times. For longer times, some estimate of the effective accuracy is provided by monitoring the definite integral of $\rho = u^2 + v^2$, which is conserved in time for the continuous system. This quantity is preserved up to at least six digits throughout all our computations.

As test to our numerical scheme, we computed the NLS solution satisfying Miller and Kamvissis' initial data (3) and found agreement with their solution.

4. Description of numerical experiments

The graphs in this section are taken from numerically computed solutions of (10), (11) for four sets of initial data. For our computations we take $N = 16384$ $(= 2^{14})$, 32768, and 65536. The time step Δt varies from 10^{-5} to 2.5×10^{-6}, depending on the spatial resolution and on ϵ. The time step is chosen so that decreasing it further would not result in a noticeable change of the solution. Both the spatial and temporal resolutions are selected to achieve an accurate computation of the smallest scales.

We present here computations for four kinds of initial values $A_0(x)$ and $S_0(x)$.

(I) Zero initial phase data

$$A_0(x) = e^{-x^2}, \qquad S_0(x) = 0.$$

This set of data is very similar to the pure soliton data studied by Miller and Kamvissis: $A_0(x) = 2\,\mathrm{sech}(x)$, $S_0(x) = 0$. For Miller and Kamvissis' data, the Zakharov–Shabat operator has pure imaginary eigenvalues and the reflection coefficients are exactly zero. For our data, the eigenvalues are almost pure imaginary and the reflection coefficients are exponentially small for small ϵ.

(II) Symmetric initial data with nonzero phase

$$A_0(x) = \frac{\sinh(2x)}{\cosh^2(2x)}, \qquad S_0(x) = \frac{1}{\cosh(2x)}.$$

The eigenvalues generated by this data have been numerically studied by Bronski [3]. The eigenvalues are symmetric about the pure imaginary axis, and are located roughly on a convex "parabola" whose vertex is at the origin. The top of the "parabola" are points $0.5 - i$ and $0.5 + i$. Thus, an eigenvalue has a bigger real part if it has a larger imaginary part and different eigenvalues have distinct real parts.

(III) Nonsymmetric initial data

$$A_0(x) = \frac{1}{\cosh(x)}, \qquad S_0(x) = \frac{2x}{\cosh(2x)}.$$

This example lacks the even/odd symmetry possessed by the first two initial data. Thus, the eigenvalues are not right/left symmetric [3].

(IV) Nonanalytic initial data

$$A_0(x) = \begin{cases} 1 - |x| & \text{if } |x| < 1, \\ 0 & \text{otherwise,} \end{cases}$$

$$S_0(x) = \frac{1}{\cosh(2x)}.$$

This initial data is not analytic at $x = 0$ and $x = \pm 1$.

Figs. 1–3 picture $\rho = |\psi(x, t; \epsilon)|^2$ of the solution corresponding to the zero initial phase data on a grid of values in space–time for $\epsilon = 0.1, 0.05, 0.025$, respectively. We also computed the solution for smaller ϵ's such as $\epsilon = 0.0125$ and $\epsilon = 0.00625$, but the corresponding space–time solution surfaces with adequate graphical resolution produce too large a file to be included here. Since this NLS solution is right/left symmetric, we plot only half of the solution surface. In these figures, the quiescent and oscillatory regions are clearly recognizable and they appear to be independent of small ϵ. The number of oscillations is proportional to $1/\epsilon$, indicating that the oscillations have wavelength $O(\epsilon)$. It is predicted by the WKB analysis that the number of solitons, hence of oscillations, is in the order of $O(1/\epsilon)$. Overall, the oscillations seem to be quite regular even as ϵ decreases. This is

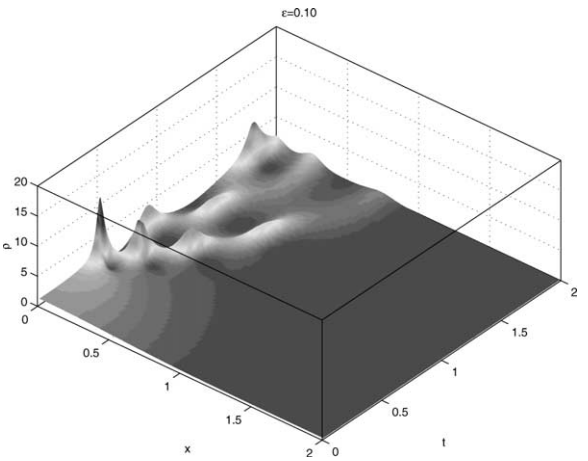

Fig. 1. Evolution of the zero initial phase data with $\epsilon = 0.10$. $N = 16384$, $\Delta t = 10^{-5}$.

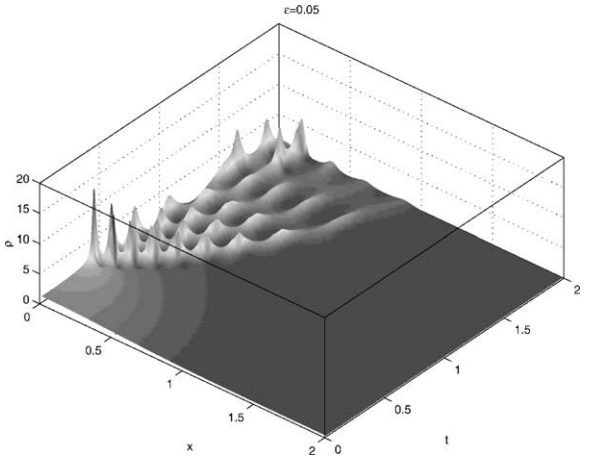

Fig. 2. Evolution of the zero initial phase data with $\epsilon = 0.05$. $N = 16384$, $\Delta t = 10^{-5}$.

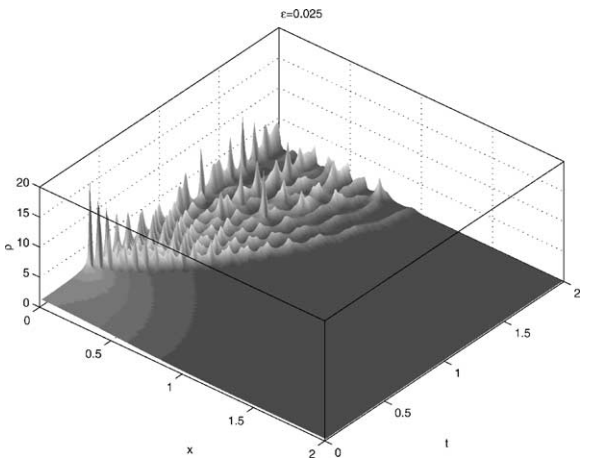

Fig. 3. Evolution of the zero initial phase data with $\epsilon = 0.025$. $N = 32768$, $\Delta t = 5 \times 10^{-6}$.

rather surprising, considering that these solitons are supposed not to separate from each other since they all have negligible speeds for tiny ϵ's. These observations are consistent with the numerical results of Miller and Kamvissis for the pure soliton solutions.

What quantities of the focusing NLS solution might converge (although perhaps weakly) as ϵ goes to zero? Eqs. (4), (5) suggest that the mass density ρ and momentum density μ are the two best candidates. To verify the weak convergence of $\rho(x,t;\epsilon)$ as $\epsilon \to 0$,

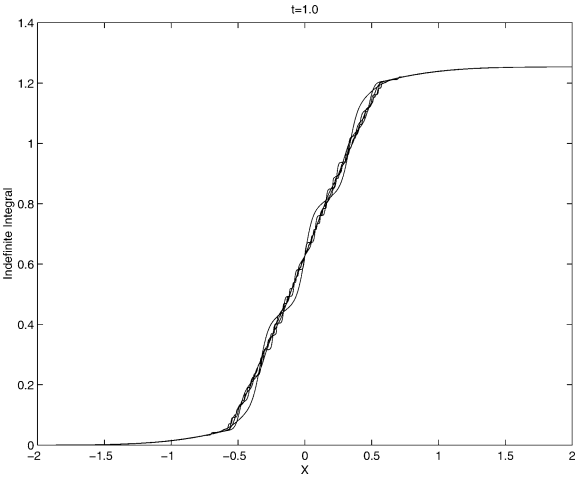

Fig. 4. Indefinite integrals of the oscillatory density $\rho(x,t,\epsilon)$ for the zero initial phase data illustrating weak convergence. Curves with more "corners" correspond to smaller ϵ's. $N = 32768$, $\Delta t = 5 \times 10^{-6}$ for $\epsilon = 0.0125$ and $N = 65536$, $\Delta t = 2.5 \times 10^{-6}$ for $\epsilon = 0.00625$.

we computed the indefinite integral

$$\int_{-\infty}^{x} \left|\psi(x',t;\epsilon)\right|^2 dx',$$

for various ϵ's. In theory, the strong convergence of the integral as ϵ goes to zero would imply the weak convergence of $\rho = |\psi(x,t;\epsilon)|^2$ with respect to x. This is motivated by the works of Lax and Levermore [22] and Venakides [29] on the zero dispersion limit of the KdV equation. Lax and Levermore wrote the KdV solution as the second spatial derivative of another function. They proved the weak convergence of the KdV solution by showing that the latter function converges strongly. Venakides improved Lax and Levermore's result by integrating once instead of twice. Finally, Goodman and Lax also used indefinite integrals to numerically verify the weak convergence in dispersive difference schemes [12].

Fig. 4 pictures the indefinite integrals at $t = 1$ for ϵ taking five different values: 0.1, 0.05, 0.025, 0.0125, and 0.00625. Curves with more "corners" correspond to smaller ϵ's. Fig. 4 clearly demonstrates the strong convergence of the indefinite integral to a function of space and time as ϵ goes to zero. As mentioned above, this implies the weak convergence of $\rho(x,t;\epsilon)$.

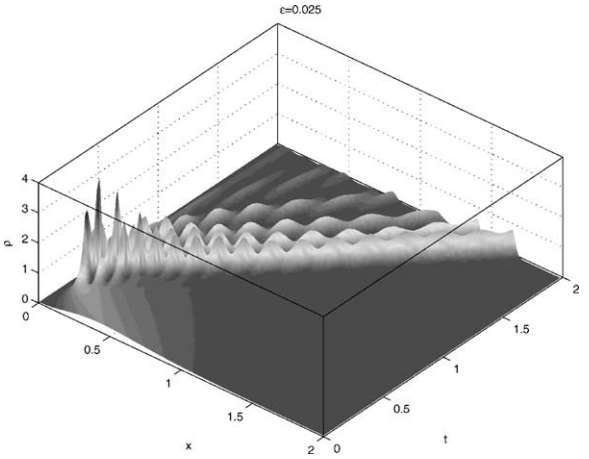

Fig. 5. Evolution of the symmetric initial data with nonzero phase with $\epsilon = 0.025$. $N = 16384$, $\Delta t = 10^{-5}$.

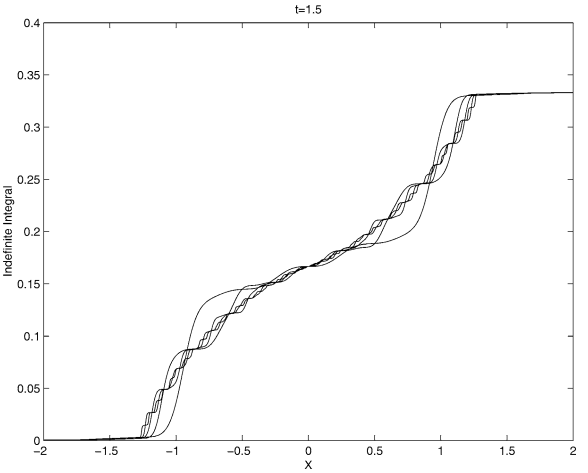

Fig. 6. Indefinite integrals of the oscillatory density $\rho(x, t, \epsilon)$ for the symmetric initial data with nonzero phase. $N = 32768$, $\Delta t = 5 \times 10^{-6}$ for $\epsilon = 0.0125$ and $N = 65536$, $\Delta t = 2.5 \times 10^{-6}$ for $\epsilon = 0.00625$.

The importance of numerically verifying the weak convergence can not be underestimated. The observation of regular patterns in oscillations alone is not enough to guarantee weak convergence. Indeed, the amplitude $|\psi(x, t; \epsilon)|$, which is the square root of $\rho(x, t; \epsilon)$, also exhibits nice patterns in oscillations as $\rho(x, t; \epsilon)$ does. We computed the indefinite integrals of the amplitude, and we did not observe any sign of convergence.

We do not include the pictures of momentum density μ in this Letter. Observe that unlike $\rho = |\psi|^2$, $\mu = -i(\epsilon/2)(\bar{\psi}\psi_x - \psi\bar{\psi}_x)$ involves spatial derivatives. Resolving the derivatives is more difficult because of the requirement of a much smaller Δx and the sensitivity of the problem to round-off noise growth. Differentiation amplifies round-off error noise.

The weak limit dynamics is an open problem. It is believed that the dynamics is described by a family of the Whitham equations, of which Eqs. (6), (7) form the first member [10,25]. In particular, the limits of ρ and μ are supposed to satisfy the latter equations in the nonoscillatory region. However, the elliptic equations (6), (7) may not have any solution for nonanalytic initial data. Whether and how nonanalyticity of the initial data may affect the existence of weak limits will be discussed later in this Letter when we study the nonanalytic initial data.

Fig. 5 pictures $\rho(x, t; \epsilon)$ over space–time for the second initial data. The parameter ϵ takes the value of 0.025. The oscillations for this initial data are the nicest and cleanest among the four initial data studied in this Letter. This is because the solitons in this case have the simplest behavior: taller soliton always run faster than shorter ones and different solitons have distinct velocities. In view of the relation between an eigenvalue and the velocity and height of the corresponding soliton, these phenomena are predicted by the location of the eigenvalues of the Zakharov–Shabat operator. In particular, the eigenvalues with the largest real parts and imaginary parts are $0.5 - i$ and $0.5 + i$. That means that the leading solitons should roughly have speed ± 1. We see from Fig. 5 that the boundary separating the oscillatory and smooth regions has a slope roughly equal to 1, implying that the leading soliton in the figure has speed 1.

Fig. 6 pictures the indefinite integrals of $\rho(x, t; \epsilon)$ for the second initial data at $t = 1.5$. The parameter ϵ takes the values of 0.1, 0.05, 0.025, 0.0125, and 0.00625. Again, curves with more "corners" correspond to smaller ϵ's. Still, we see strong convergence in the integrals.

Fig. 7 pictures $\rho(x, t; \epsilon)$ at $\epsilon = 0.025$ for the nonsymmetric initial data. Since the solution is not left/right symmetric, we plot the solution surface for $x \in [-2, 2]$. We see from the pictures that the oscillations are first generated from the right at about $t = 0.25$. Later, at approximately $t = 0.8$, new oscillations come out from the left. These two wave trains begin to inter-

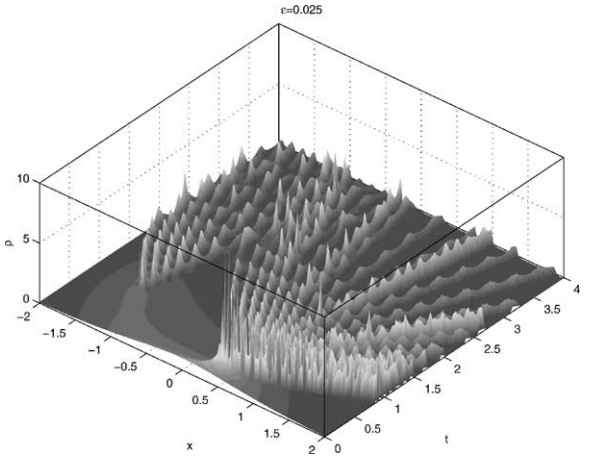

Fig. 7. Evolution of the nonsymmetric initial data exhibiting the interaction of two wave trains with $\epsilon = 0.025$, $N = 32768$, $\Delta t = 5 \times 10^{-6}$.

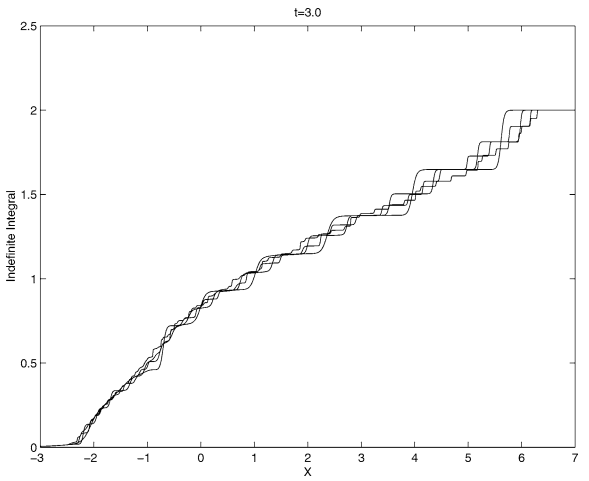

Fig. 8. Indefinite integrals of the oscillatory density $\rho(x, t, \epsilon)$ for the nonsymmetric initial data. $N = 32768$, $\Delta t = 5 \times 10^{-6}$ for $\epsilon = 0.0125$.

act at $t = 2$. The oscillations appear to be quite regular before and even during the interaction.

Fig. 8 pictures the indefinite integrals of the nonsymmetric solution at $t = 3$ for ϵ equal to 0.1, 0.05, 0.025, and 0.0125. Time $t = 3$ is during the interaction of the two wave trains. Strong convergence in the indefinite integral is clear at $t = 3$. Therefore, the density $\rho(x, t; \epsilon)$ still converges weakly even during the interaction of the two trains of solitons.

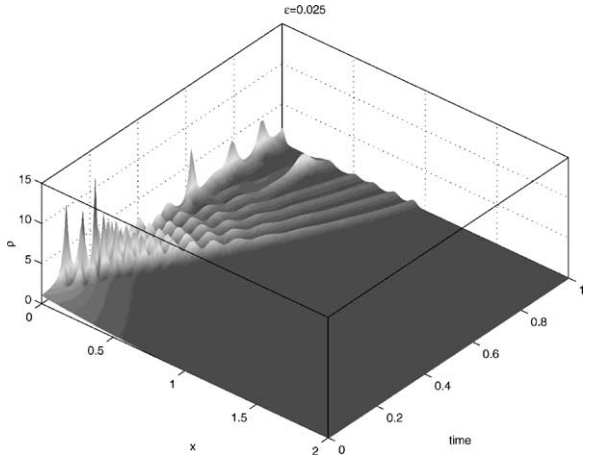

Fig. 9. Evolution of the nonanalytic initial data with $\epsilon = 0.025$, $N = 32768$, $\Delta t = 5 \times 10^{-6}$.

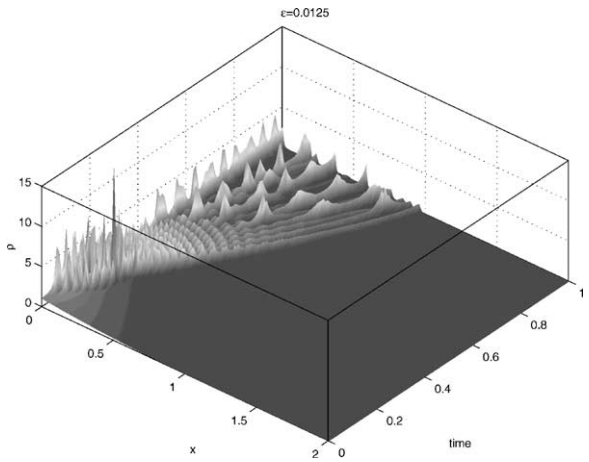

Fig. 10. Evolution of the nonanalytic initial data with $\epsilon = 0.0125$, $N = 32768$, $\Delta t = 5 \times 10^{-6}$.

Figs. 9–11 picture $\rho(x, t; \epsilon)$ for the nonanalytic initial data. This time, $\epsilon = 0.025$, 0.0125, and 0.00625. Contrary to what many people expect [4], the oscillations appear to be quite regular even for small ϵ. What is striking about this data is that the oscillatory region in space–time is seemed to approach the origin at the initial line $t = 0$ as ϵ goes to zero. This phenomenon can be explained by Eqs. (6), (7). Indeed, the initial value problem for these equations has no local solution in the neighborhood of the origin. This follows from the fact that Eqs. (6), (7) are elliptic when $\rho \neq 0$

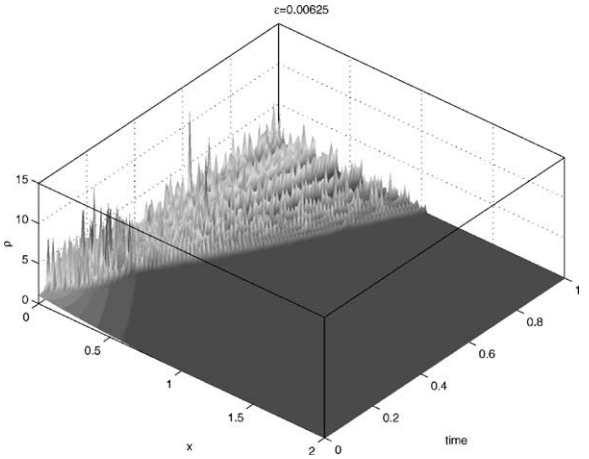

Fig. 11. Evolution of the nonanalytic initial data with $\epsilon = 0.00625$, $N = 65536$, $\Delta t = 2.5 \times 10^{-6}$.

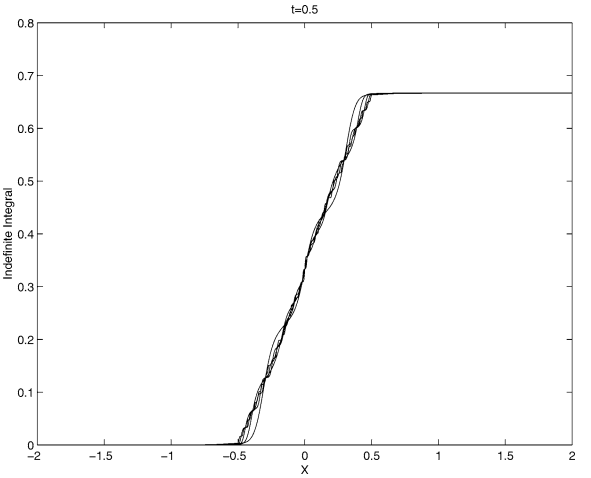

Fig. 12. Indefinite integrals of the oscillatory density $\rho(x,t,\epsilon)$ for the nonanalytic initial data. $\epsilon = 0.10$, 0.05, 0.025, 0.0125, and 0.00625.

and that the initial data

$$\rho(x,0) = \begin{cases} (1-|x|)^2 & \text{if } |x|<1, \\ 0 & \text{otherwise} \end{cases}$$

has no derivative at $x = 0$.

Interestingly, Eqs. (6), (7) can also be used to explain why the oscillatory region does not touch the initial line at $x = \pm 1$, which are the other two nonanalytic points in the initial data. The main reason is that the initial value problem of (6), (7) has local C^1 solutions in the neighborhood of $x = \pm 1$. To see this, observe that Eqs. (6), (7) lose ellipticity when $\rho = 0$ and that they have a trivial solution $\rho = 0$. Initially, $\rho(x,0)$ is positive for $|x| < 1$, zero for $|x| \geqslant 1$ and C^1 smooth at $x = \pm 1$. To obtain a local C^1 solution of (6), (7) in the neighborhood of, say, $x = 1$, one needs to connect the trivial $\rho = 0$ solution from the right to the nontrivial $\rho > 0$ solution from the left. More precisely, we introduce

$$A_t + vA_x + \frac{1}{2}Av_x = 0, \tag{14}$$

$$v_t + vv_x - 2AA_x = 0, \tag{15}$$

which are obtained from Eqs. (6), (7) after the substitution $\rho = A^2$. The initial data $A(x,0) = 1 - |x|$ if $|x| < 1$ and vanishes otherwise, and $v(x,0) = S_0'(x)$ everywhere. We first continue analytically the solution $A(x,t)$, $v(x,t)$ of (14), (15) from the left to the right of $x = 1$ by extending $A(x,0)$ analytically across $x = 1$; the initial data then becomes $A(x,0) = 1 - x$ in the neighborhood of $x = 1$. For each small $t > 0$, $A(x,t)$ strictly decreases from positive to negative values as x increases in the neighborhood of $x = 1$ because $A(x,0)$ has the same monotonicity initially. Hence, the loci of zeros of $A(x,t)$ form a curve $x = x^*(t)$ in the vicinity of $x = 1$ and $t = 0$. $A(x,t)$ is then positive when $x < x^*(t)$ and negative when $x > x^*(t)$. We then connect the trivial solution $A(x,t) = 0$ of (14), (15) from the right to the positive solution $A(x,t)$ from the left along the curve $x = x^*(t)$ and leave $v(x,t)$, obtained from the previous analytic continuation, intact. Accordingly, $\rho(x,t) = A^2(x,t)$ will be C^1 smooth at each point on the curve $x = x^*(t)$. In this way, Eqs. (6), (7) are shown to have a local C^1 solution in the neighborhood of $x = 1$ satisfying the initial conditions.

Finally, Fig. 12 pictures the indefinite integrals of $\rho(x,t;\epsilon)$ for the nonanalytic initial data at $t = 0.5$. The parameter ϵ takes the values of 0.1, 0.05, 0.025, 0.0125, and 0.00625. Strong convergence in the integrals is obvious. This gives solid evidence for the existence of weak limit even when the initial data is not analytic.

5. Conclusion

The generation and propagation of oscillations is an important natural phenomenon for "nearly unstable" nonlinear dispersive equations. Since the under-

lying initial value problem with zero dispersion is unstable, the analytical and even numerical study of the small dispersion problem has proved to be a road hard to travel. In this Letter, we have developed a numerical scheme to compute the solution of the focusing NLS with small dispersion. We are able to resolve some of the fine micro-structure of the oscillations. We observe quiescent regions in space and time coexisting with regions of rather regular oscillations. For all the initial data we experimented, it is enough to smooth oscillations solely in space to capture weak convergence of the solution. If true for other initial data, it would be interesting to develop an analytical approach, implementing this observation, to study the weak limit.

Acknowledgements

We would like to thank Thomas Y. Hou for valuable discussions. We are also grateful to referees for interesting comments.

References

[1] A.M. Bloch, Y. Kodama, in: N. Ercolani, I. Gabitov, D. Levermore, D. Serre (Eds.), Singular Limits of Dispersive Waves, in: NATO ARW Series B: Physics, Vol. 320, Plenum, New York, 1994, pp. 1–19.
[2] J.C. Bronski, D.W. McLaughlin, in: N. Ercolani, I. Gabitov, D. Levermore, D. Serre (Eds.), Singular Limits of Dispersive Waves, in: NATO ARW Series B: Physics, Vol. 320, Plenum, New York, 1994, pp. 21–38.
[3] J.C. Bronski, Physica D 97 (1996) 376.
[4] J.C. Bronski, J.N. Kutz, Phys. Lett. A 254 (1999) 325.
[5] R.E. Caflisch, O.F. Orellana, SIAM J. Math. Anal. 20 (1989) 293.
[6] P. Deift, K.T.-R. McLaughlin, Mem. Amer. Math. Soc. 131 (1998) 624.
[7] B.A. Dubrovin, S.P. Novikov, Russian Math. Surveys 44 (1989) 35.
[8] N. Ercolani, S. Jin, D. Levermore, W. MacEvoy, The zero dispersion limit of the NLS/mKdV hierarchy for the nonselfajoint ZS operator, preprint, 1993.
[9] H. Flaschka, M.G. Forest, D.W. McLaughlin, Commun. Pure Appl. Math. 33 (1980) 739.
[10] M.G. Forest, J. Lee, in: J.L. Ericksen, D. Kinderlehrer, M. Slemrod (Eds.), Oscillation Theory, Computation and Method of Compensated Compactness, Springer, 1986, pp. 35–69.
[11] M.G. Forest, K. T-R McLaughlin, J. Nonlinear Sci. 8 (1998) 43.
[12] J. Goodman, P.D. Lax, Commun. Pure Appl. Math. 41 (1988) 591.
[13] A.V. Gurevich, L.P. Pitaevskii, Sov. Phys. JETP 38 (1974) 291.
[14] H. Hasimoto, J. Fluid Mech. 51 (1972) 477.
[15] T.Y. Hou, P.D. Lax, Commun. Pure Appl. Math. 44 (1991) 1.
[16] T.Y. Hou, J.S. Lowengrub, M.J. Shelley, J. Comput. Phys. 114 (1994) 312.
[17] S. Jin, C.D. Levermore, D.W. McLaughlin, in: N. Ercolani, I. Gabitov, D. Levermore, D. Serre (Eds.), Singular Limits of Dispersive Waves, in: NATO ARW Series B: Physics, Vol. 320, Plenum, New York, 1994, pp. 235–255.
[18] S. Jin, C.D. Levermore, D.W. McLaughlin, Commun. Pure Appl. Math. 52 (1999) 613.
[19] S. Kamvissis, K. McLaughlin, P. Miller, Semiclassical soliton ensembles for the focusing nonlinear Schrödinger equation, preprint, 2000.
[20] Y. Kodama, S. Wabnitz, Opt. Lett. 20 (1995) 2291.
[21] R. Krasny, J. Fluid Mech. 167 (1986) 65.
[22] P.D. Lax, C.D. Levermore, Commun. Pure Appl. Math. 36 (1983) 253, 571, 809.
[23] P.D. Lax, C.D. Levermore, S. Venakides, in: T. Fokas, V.E. Zakharov (Eds.), Important Developments in Soliton Theory 1980–1990, Springer, Berlin, 1992.
[24] C. Peskin, D. McQueen, Am. J. Physiol. 266 (1994) H319.
[25] P. Miller, S. Kamvissis, Phys. Lett. A 247 (1998) 75.
[26] J.E. Rothenberg, D. Grischkowsky, Phys. Rev. Lett. 62 (1989) 531.
[27] R.Z. Sagdeev, in: M.A. Leontovich (Ed.), in: Reviews of Plasma Physics, Vol. 4, Consultants Bureau, New York, 1966, pp. 23–91.
[28] F.R. Tian, J. Ye, Commun. Pure Appl. Math. 52 (1999) 655.
[29] S. Venakides, Amer. Math. Soc. Trans. 301 (1987) 189.
[30] G.B. Whitham, Linear and Nonlinear Waves, Wiley, New York, 1974.
[31] V. Zakharov, A. Shabat, Sov. Phys. JETP 34 (1972) 62.